



# Core-shell Ag@Pt nanoparticles supported on sepiolite nanofibers for the catalytic reduction of nitrophenols in water: Enhanced catalytic performance and DFT study

Ying Ma <sup>a,b</sup>, Xiaoyong Wu <sup>a</sup>, Gaoke Zhang <sup>a,\*</sup>

<sup>a</sup> Hubei Provincial Collaborative Innovation Center for High Efficient Utilization of Vanadium Resources, State Key Laboratory of Silicate Materials for Architectures, School of Resources and Environmental Engineering, Wuhan University of Technology, Wuhan 430070, PR China

<sup>b</sup> Center for Circular Economy and Clean Production, South China Institute of Environmental Sciences, Ministry of Environmental Protection of the People's Republic of China, Guangzhou 510655, PR China

## ARTICLE INFO

### Article history:

Received 1 November 2016

Received in revised form

28 November 2016

Accepted 8 December 2016

Available online 9 December 2016

### Keywords:

Ag@Pt Nanoparticles

Sepiolite nanofibers

Core-shell structure

DFT Calculations

Catalytic reduction of nitrophenols

## ABSTRACT

We reported the enhanced catalytic property of core-shell Ag@Pt nanoparticles supported on sepiolite nanofibers for the reduction of nitrophenols in the presence of NaBH<sub>4</sub>. Furthermore, we confirmed the contribution of core-shell structure to the enhanced catalytic performance of Ag@Pt nanoparticles by DFT calculations. The Ag@Pt/sepiolite catalysts were prepared using a successive reduction method, in which core-shell Ag@Pt nanoparticles were highly dispersed on sepiolite nanofibers. DFT calculations showed that the charge redistribution and *s-d* hybridization between Ag cores and Pt shells contributed to the unique electronic structure of Ag@Pt nanoparticles. More importantly, 2 wt.% Ag@Pt/sepiolite catalyst exhibited much higher catalytic activity toward nitrophenols reduction than Ag/sepiolite and Pt/sepiolite, and relatively high catalytic stability even after 5 cycles. The enhanced catalytic performance of Ag@Pt/sepiolite catalysts was primarily owing to the large surface area and high porosity of sepiolite nanofibers and the unique electronic structure of core-shell Ag@Pt nanoparticles, which resulted in the effective adsorption of nitrophenols and the electron transfer from BH<sub>4</sub><sup>-</sup> to nitrophenols, respectively. This study probably provides new insights into the catalytic reduction of nitrophenols in water by forming the composite between bimetallic core-shell nanoparticles and natural low-cost supports.

© 2016 Elsevier B.V. All rights reserved.

## 1. Introduction

Nitrophenols, including para-, meta- and ortho-nitrophenol (PNP, MNP and ONP) are one kind of hazardous and toxic pollutants derived from the manufacture of pesticides, pharmaceuticals and synthetic dyes. The untreated discharge of nitrophenols would directly poison the aquatic organisms and indirectly cause multiple health problems to human being [1]. However, it's difficult to remove the soluble and stable nitrophenols efficiently and completely through the traditional wastewater treatment [2,3]. The catalytic reduction of nitrophenols has gradually been the focus of wastewater treatment, because the toxic nitrophenols could be completely reduced to beneficial aminophenols in short time with the acceleration of various catalysts [4,5].

Bimetallic nanoparticles, especially with core-shell structure have received extensive attention and become one of the most promising candidates for catalysis due to their fascinating activity, selectivity, stability and resistance to poisoning as compared to monometallic counterparts [6–8]. For instance, Rh@Pt core-shell catalyst exhibited better catalytic performances than RhPt alloy and Rh + Pt monometallic nanoparticles for the preferential oxidation of CO in H<sub>2</sub> at 70 °C [9]. Pt-based and Ag-based bimetallic catalysts were synthesized to catalyze the reduction of nitrophenols and exhibited favorable catalytic performance. The catalytic performance of the Pt-Ni alloys was superior to that of monometallic Pt nanoparticles [10]. The Au-Ag alloy nanoparticles loaded on graphene oxide (GO) showed better catalytic performance for the reduction of PNP than either Ag or Au nanoparticles alone nanoparticles loaded on (GO) [11]. Pt-Ag bimetallic nanoparticles and core-shell Ag@Pt nanoparticles were also synthesized, and their physicochemical properties, such as catalytic oxidation, catalytic reduction, H<sub>2</sub> production and electrocatalytic effect, were studied [12–14]. However, the role of core-shell structure in the

\* Corresponding author.

E-mail address: [gkzhang@whut.edu.cn](mailto:gkzhang@whut.edu.cn) (G. Zhang).

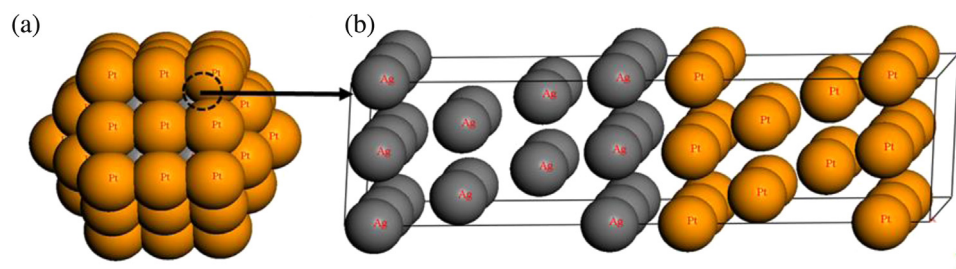


**Fig. 1.** Simulated structure of Ag@Pt nanoparticles (a) and 2 × 2 layer of Pt (111) and Ag (111) surfaces (b).

catalytic reduction of nitrophenols over Ag@Pt nanoparticles has rarely been investigated, and is still expected to be understood by theoretic calculations.

Meanwhile, it's would be meaningful to synthesize supported Ag@Pt nanoparticles as mentioned above to decrease the noble metal consumptions and enhance their catalytic performance during the reduction of nitrophenols in water. Noble metals nanoparticles are generally loaded on substrates such as  $\text{Al}_2\text{O}_3$ ,  $\text{SiO}_2$  and  $\text{TiO}_2$  in heterogeneous catalysis to improve the catalytic activity, recovery and flexibility [15,16]. In addition, natural clays with unique morphology and structure as the substrate of noble metal nanoparticles have gradually drawn much attention due to their low cost, material availability and environmental friendliness [17–19]. Sepiolite,  $(\text{Si}_{12}\text{Mg}_{8}\text{O}_{30})(\text{OH})_4(\text{OH})_2 \cdot 8\text{H}_2\text{O}$ , is a typically natural clay minerals with fiber shape, the structure of which was composed of two discontinuous tetrahedral silica sheets and a central magnesia sheet, and developed into interior tunnels and alternation blocks grown in fiber direction [20]. The tunnel structure resulted from the discontinuity of the silica sheets led to huge specific surface area and high porosity of sepiolite fibers, which can provide more reaction sites for catalytic activity and prevent nano-catalysts from aggregation [21,22]. Therefore, the catalytic activity, recyclability, and flexibility of sepiolite supported catalysts would be further enhanced due to the unique structure and morphology. For instance,  $\text{TiO}_2$ /sepiolite catalyst presented enhanced photocatalytic activity for the degradation of lignin, phenol and other organic pollutants in wastewater [23,24]. Pd-sepiolite showed higher catalytic activity for the carbon–carbon coupling reaction than unsupported Pd and Pd- $\text{SiO}_2$  [25]. However, bimetallic core-shell nanoparticles loaded on sepiolite nanofibers for the catalytic reduction of nitrophenols are hardly investigated.

In this work, core-shell Ag@Pt nanoparticles were highly dispersed on sepiolite nanofibers to prepare Ag@Pt/sepiolite catalysts by a successive reduction method. Theoretical calculations were introduced to verify the contribution of the Ag@Pt core-shell structure to the enhancement of the catalytic performance. The catalytic performance of Ag@Pt/sepiolite for the reduction of nitrophenols (PNP, ONP and MNP) with  $\text{NaBH}_4$  as reducing agent was investigated in water. The effects of Ag@Pt nanoparticles loading and the molar ratio of Ag to Pt (Ag: Pt) on the catalytic performance were further analyzed to optimize the Ag@Pt/sepiolite catalyst. In addition, the kinetics and mechanism of the catalytic reduction of nitrophenols over Ag@Pt/sepiolite catalyst were discussed.

## 2. Experimental

### 2.1. Materials

Hexachloroplatinic acid ( $\text{H}_2\text{PtCl}_6 \cdot 6\text{H}_2\text{O}$ ), silver nitrate ( $\text{AgNO}_3$ ), sodium citrate, polyvinylpyrrolidone (PVP), ascorbic acid and other reagents used in the work were all of analytical grade and purchased from the China National Medicines Company. The pristine sepiolite was from Henan Province (China), which was pretreated

for further use as follows [26]: First of all, the raw sepiolite was added into deionized water to form a sepiolite suspension (20 g/L) followed by stirring for 24 h. After that, the above suspension was filtered and rinsed three times by deionized water. Before milled through a 60-mesh sieve, the obtained powders were dried at 105 °C for 2 h. Finally, the sepiolite products were further ultrasonically dispersed into the deionized water for the following synthesis of Ag@Pt/sepiolite catalysts.

### 2.2. Synthesis of catalyst

The Ag@Pt/sepiolite catalysts were synthesized by a successive reduction method with  $\text{H}_2\text{PtCl}_6 \cdot 6\text{H}_2\text{O}$  and  $\text{AgNO}_3$  as platinum and silver precursor, respectively. In a typical synthesis, silver precursor,  $\text{AgNO}_3$  (0.527 mL, 10 mg/mL) was firstly reduced by ascorbic acid (10 mL, 5.4 mg/mL) for 30 min under magnetic stirring at 80 °C. Platinum precursor,  $\text{H}_2\text{PtCl}_6 \cdot 6\text{H}_2\text{O}$  (3.2 mL, 10 mg/mL) was then reduced by ascorbic acid (10 mL, 21.6 mg/mL) for 1 h under magnetic stirring at 80 °C. The red silver colloid turned into dark one, indicating that the silver cores were coated with platinum shells. Afterwards, sepiolite nanofibers suspension (0.9393 g sepiolite) was added into the colloid with further stirring for 4 h. 0.45 g of sodium citrate and 0.17 g of PVP as protective and dispersant components existed in the whole reduction of platinum and silver precursors. Finally, the mixed suspension was separated by centrifuging, washed with deionized water and then dried at 50 °C for 12 h under vacuum to obtain 2 wt.% Ag@Pt/sepiolite catalyst (Ag: Pt = 1:1). Samples with different nominal weights of Ag@Pt nanoparticles (0, 1, 2 and 4 wt.%) and different Ag: Pt (1:1, 1:2, 2:1) were prepared in the study.

### 2.3. Materials characterization

X-ray diffraction (XRD) measurements were performed to analyze the phase composition and structure of the Ag@Pt/sepiolite catalyst on Rigaku D/max-RB diffractometer with  $\text{Cu K}\alpha$  radiation. The morphology and structure of the Ag@Pt/sepiolite composites were measured by transmission electron microscopy (TEM) along with high-resolution transmission electron microscopy (HRTEM) (JEM 2100F microscope). The pore structure and specific surface area of samples were analyzed by the nitrogen adsorption-desorption isotherms on Micromeritics ASAP 2020 automatic equipment. The surface atom status of samples was analyzed by X-ray photoelectron spectroscopy (XPS) (VG Multilab 2000). The bond structure of the samples was studied by Fourier-transform infrared (FTIR) using Thermo Scientific Nicolet6700 FTIR spectrometer.

### 2.4. DFT calculations

In order to theoretically understand the interaction and electronic structure of Pt shells and Ag cores in Ag@Pt nanoparticles, the first-principles density functional theory (DFT) was applied to perform all of the calculations using DMol<sup>3</sup> code [27–29]. The

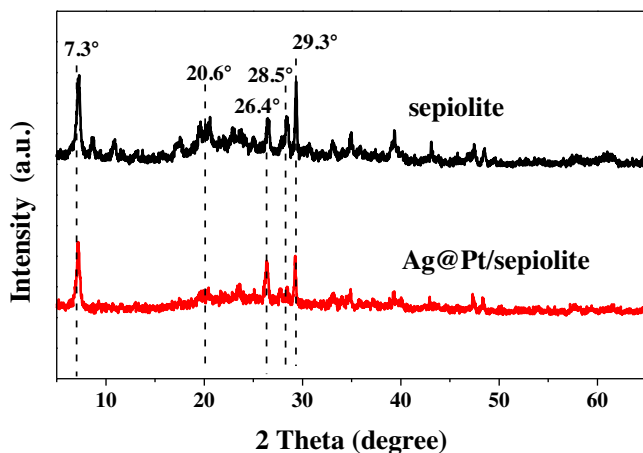


Fig. 2. XRD patterns of sepiolite and Ag@Pt/sepiolite catalyst.

exchange-correlation effects were depicted by the generalized gradient approximation (GGA) along with the Perdew-Burke-Ernzerhof (PBE) functional [30]. The all electron relativistic (AER) core treat method and double numeric plus polarization (DNP) basis set were taken for the calculation accuracy and description of electronic wave functions, respectively [31,32]. Meanwhile, the convergence tolerance was  $1.0 \times 10^{-5}$  Ha, and the maximum were 0.002 Ha/Å for the forces and 0.005 Å for the displacement. In this study, a  $2 \times 2$  layer of Pt (111) and Ag (111) surfaces (Fig. 1) was taken to simulate the interfaces of Pt shells and Ag cores in Ag@Pt nanoparticles. The optimization of the structure was performed to ensure its reliability with the same methods and parameters in previous studies [33,34]. For all calculations, the k-point was set to  $2 \times 2 \times 1$  for the  $2 \times 2$  layer of Pt (111) and Ag (111) surfaces.

## 2.5. Catalytic activity tests

The catalytic reduction of nitrophenols (PNP, ONP and MNP) was carried out in a reactor with a volume of 500 mL. Firstly, fresh NaBH<sub>4</sub> solution (40 mM, 10 mL) and nitrophenols solution (0.2 mM, 100 mL) were added to reactor under constant stirring. Next, 0.1 g of Ag@Pt/sepiolite was put in the above mixture, and then the samples were gathered at an interval of reaction time (0, 1, 2, 5, 8, 10, 12 and 15 min). Finally, the concentrations of nitrophenols and aminophenols in the collected samples were monitored on Thermo Scientific 8000 UV-vis spectrophotometer. Moreover, the used catalyst was gathered, washed with deionized water and then dried in vacuum for the cycling catalytic tests.

## 3. Results and discussion

### 3.1. Characterization of catalysts

As presented in Fig. 2, the main diffraction peaks at  $2\theta = 7.3^\circ$  (110),  $20.6^\circ$  (131),  $26.4^\circ$  (080) and  $28.5^\circ$  (331) of the samples were indexed to the characteristic peaks of natural sepiolite (JCPDS, No. 75-1597), while the peak at  $2\theta = 29.3^\circ$  was possibly attributed to the characteristic peak of calcium carbonate (JCPDS, No. 86-0174) [20,35]. Furthermore, the characteristic peaks of metallic Pt and Ag cannot be found in the pattern of the sample, owing to the low content of Ag@Pt nanoparticles in the composite. In addition, the relative peaks of sepiolite in Ag@Pt/sepiolite is slightly lower than that of pure one, probably resulting from the Ag@Pt nanoparticles deposition and pretreatment [36].

TEM and HRTEM images (Fig. 3a–b) of Ag@Pt/sepiolite catalyst illustrate that Ag@Pt nanoparticles with a diameter of 30–50 nm

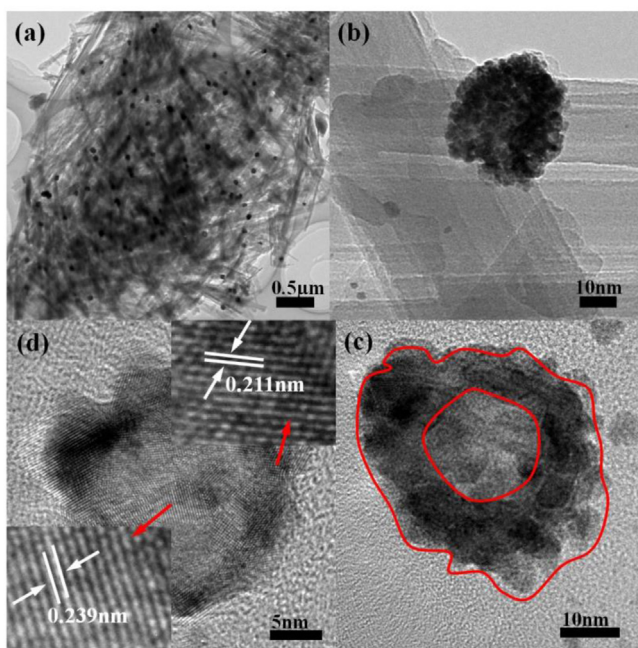


Fig. 3. TEM and HRTEM images of Ag@Pt/sepiolite catalyst ((a) and (b)) and Ag@Pt colloid ((c) and (d)).

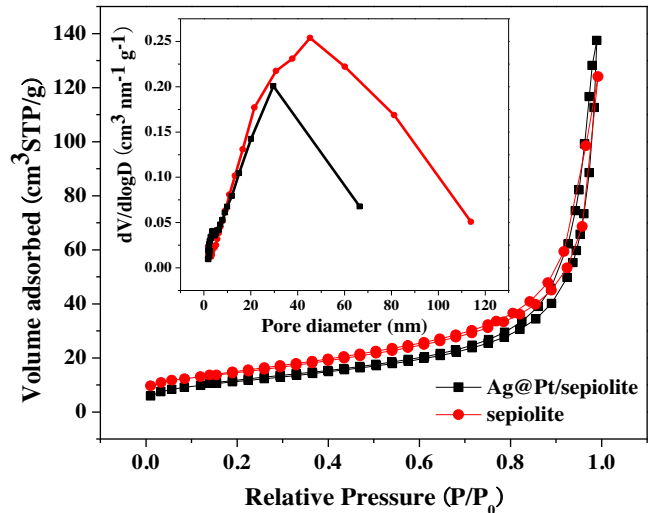
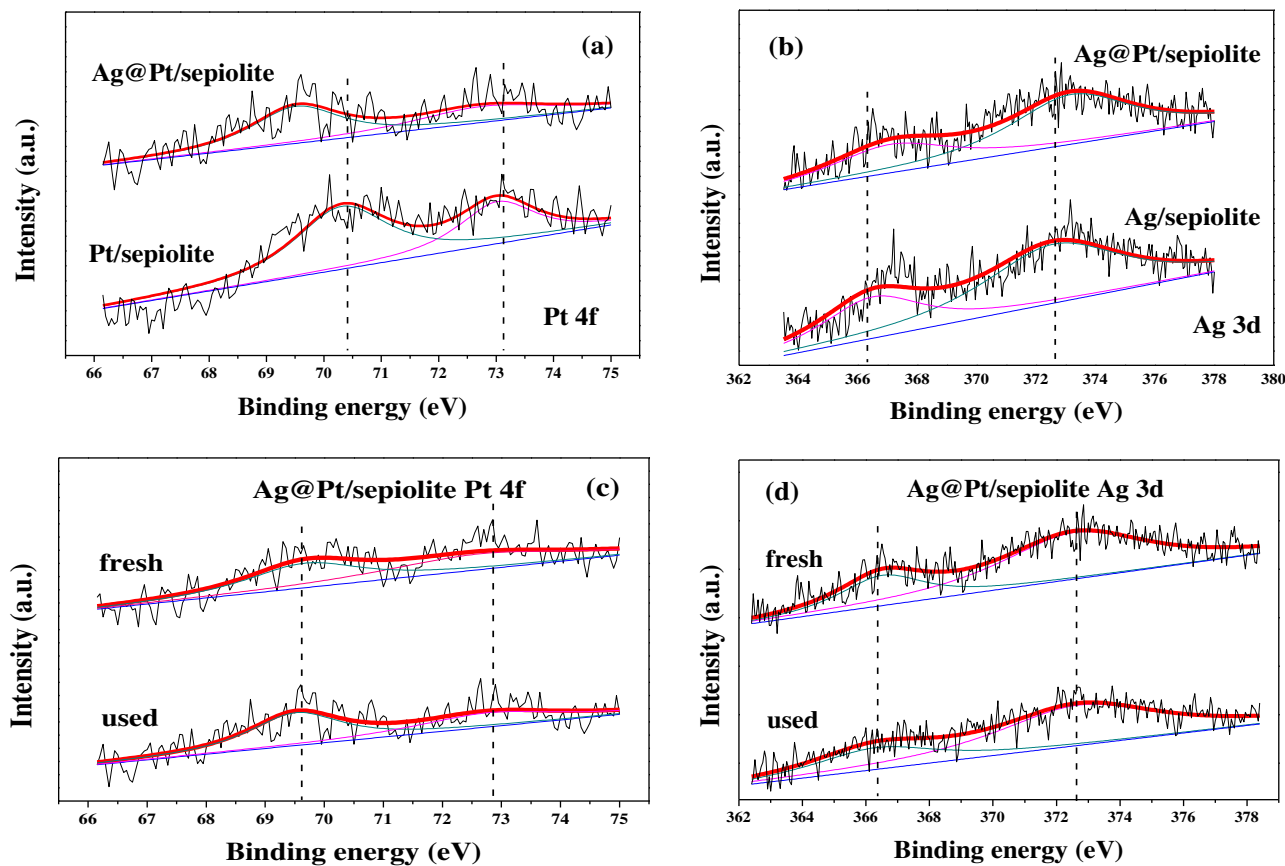


Fig. 4. Nitrogen adsorption-desorption isotherms and pore size distribution curves (inset) of sepiolite and Ag@Pt/sepiolite catalyst.

in spherical or elliptical shape are highly dispersed on sepiolite nanofibers. Furthermore, the core-shell structure of Ag@Pt nanoparticles is revealed through the HRTEM images of Ag@Pt colloid. The lighter Ag cores are coated with the darker Pt shells in the red region of Fig. 3c, which indicates the existence of Ag@Pt nanoparticles with core-shell structure [37,38]. The measured lattice spacing in the edge region is 0.211 nm, corresponded to the (111) facet of Pt crystals; the lattice spacing in the interior region is 0.239 nm, attributed to the (111) facet of Ag crystals (Fig. 3d), further demonstrating the presence of Ag@Pt core-shell structure [39,40]. The superior catalytic activity of Ag@Pt nanoparticles was mainly attributed to the Ag@Pt core-shell structure [41].

The nitrogen adsorption-desorption isotherms of samples were displayed in Fig. 4. All isotherms of the samples were belonged to the typical type IV adsorption-desorption isotherm with a hysteresis loop type H3, indicating the existence of slitlike pores and



**Fig. 5.** High resolution XPS spectra of the Ag@Pt/sepoltite catalyst: (a) Pt 4f, compared with Pt/sepoltite, (b) Ag 3d, compared with Ag/sepoltite, (c) Pt 4f, fresh and used ones and (d) Ag 3d, fresh and used ones.

mesopores in samples [42]. The inset pore size distribution lines also confirmed that the pore size distributions of two samples were mainly located on ca. 45 and ca. 35 nm, respectively. It's demonstrated that the loading of Ag@Pt nanoparticles rarely affected the sepoltite structure. As presented in Table 1, the BET surface area was decreased after the deposition of Ag@Pt/sepoltite nanoparticles due to the partly blocking of pores and tunnels [43]. The  $S_{BET}$  of 2 wt.% Ag@Pt/sepoltite is a little bit larger than that of other Ag@Pt/sepoltite catalysts, which might be attributed to the intercalation of Ag@Pt nanoparticles into sepoltite interlayer, bringing about some smaller pores [44]. Generally, larger specific surface area can provide much more active sites and adsorption interface for the catalytic reduction of nitrophenols.

The XPS analysis results of Ag@Pt/sepoltite catalysts are showed in Fig. 5. The Pt 4f spectra of Ag@Pt/sepoltite (Fig. 5a) could be deconvoluted into a pair of doublets at 69.7 eV and 72.6 eV, consistent with Pt  $4f_{7/2}$  and Pt  $4f_{5/2}$  of metallic Pt, and that of Pt/sepoltite with identical Pt loading are at 70.3 eV and 73.2 eV [45]. The doublets in Ag 3d spectra of Ag@Pt/sepoltite (Fig. 5b) are at 367.1 eV and 373.2 eV, consistent with the Ag  $3d_{5/2}$  and Ag  $3d_{3/2}$  of metallic Ag, and the corresponding doublets of Ag/sepoltite with identical Ag loading are at 366.5 eV and 372.6 eV [46]. All peaks in Pt

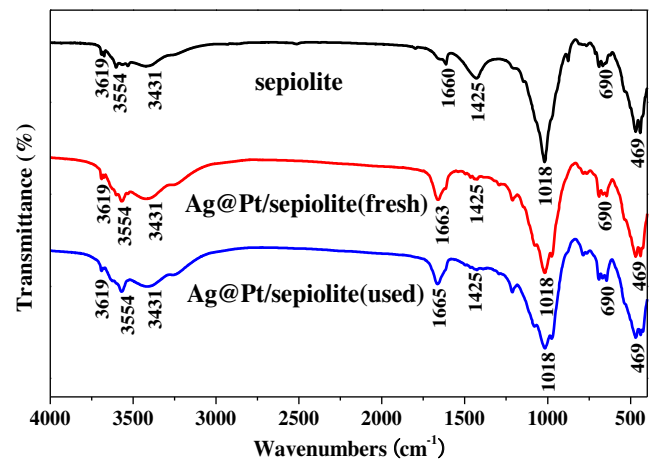


**Fig. 6.** FTIR spectra of sepoltite, fresh and used Ag@Pt/sepoltite catalysts for catalytic reduction of PNP.

4f and Ag 3d spectra of Ag@Pt/sepoltite presented an energy shift of 0.6 eV compared to that of Pt/sepoltite and Ag/sepoltite, respectively, which denotes the unusual electronic structure of Pt shells and Ag cores in Ag@Pt nanoparticles due to the electron transfer from Ag to Pt atoms and strain effect of Ag cores imposed on Pt shells [47,48]. Fig. 5c and d displays the Pt 4f and Ag 3d spectra of the fresh and used catalyst samples, respectively. The peaks of the used Ag@Pt/sepoltite catalyst scarcely changed after the catalytic reduction of PNP as compared to the fresh one, demonstrating that Ag@Pt/sepoltite possesses well catalytic stability.

**Table 1**

Textural parameters of Ag@Pt/sepoltite with different Ag@Pt loadings.

Sample	$S_{BET}$ (m <sup>2</sup> /g)	$V_p$ (cm <sup>3</sup> /g)	$d_p$ (nm)
sepoltite	49	0.213	20.91
1 wt.% Ag@Pt/sepoltite	41	0.183	18.06
2 wt.% Ag@Pt/sepoltite	42	0.224	17.28
4 wt.% Ag@Pt/sepoltite	40	0.187	17.32

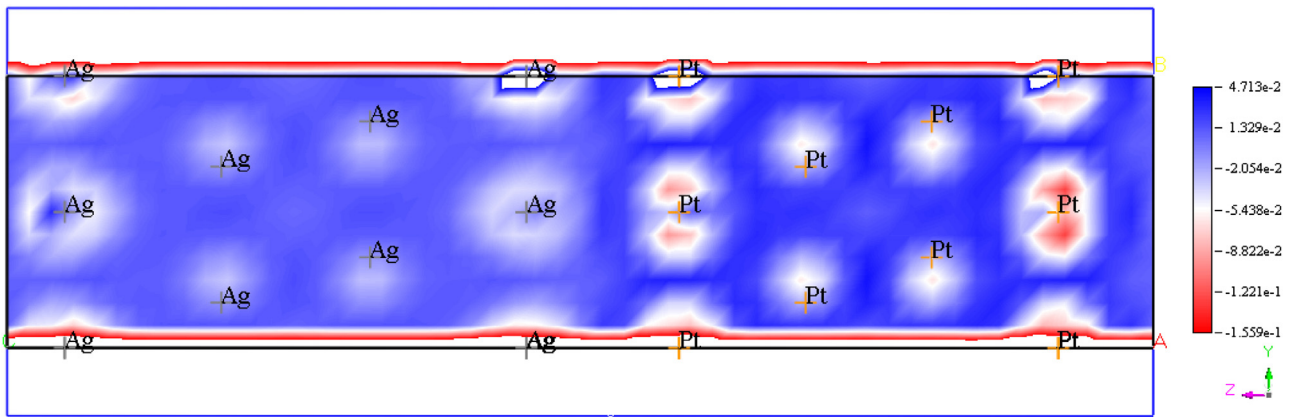


**Fig. 7.** Electron deformation density of the  $2 \times 2$  layer of Pt (111) and Ag (111) surfaces, and the loss and gain of electrons are indicated in blue and red, respectively. (For interpretation of the references to colour in this figure legend, the reader is referred to the web version of this article.)

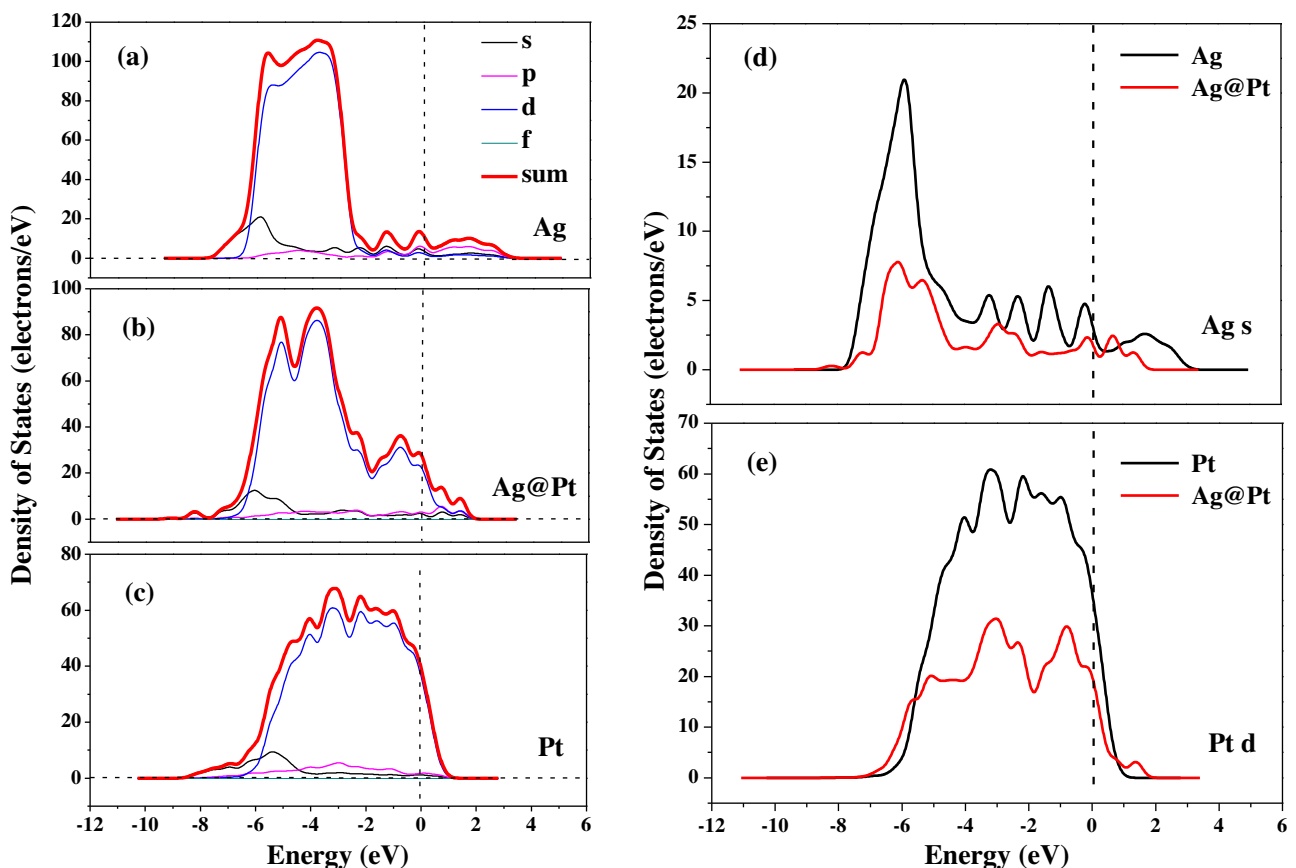


**Fig. 8.** The TDOS and partial density of states (PDOS) of Ag (a), Ag@Pt (b) and Pt (c) nanoparticles, the  $s$ -electron PDOS of Ag cores (d) and the  $d$ -electron PDOS of Pt shells (e), respectively.

**Fig. 6** shows the FTIR spectra of the pure sepiolite, fresh and recovered Ag@Pt/sepiolite composites for the catalytic reduction of PNP. The weak peaks at 3619, 3554 and  $690\text{ cm}^{-1}$  in the samples are corresponding to the stretching and bending vibrations of  $\text{Mg}_3\text{OH}$  in the octahedral sheet [49]. While the Si–O coordination peak at  $1018\text{ cm}^{-1}$  belongs to Si–O stretching vibrations in tetrahedral silica sheets, and the band at  $469\text{ cm}^{-1}$  is also ascribed to Si–O–Si bending vibrations [50]. From those, it can be found that the deposition of Ag@Pt nanoparticles hardly affected the structure of sepiolite nanofibers. In addition, the bands at 3431 and  $1660$  ( $1663, 1665\text{ cm}^{-1}$ ) in the spectra are assigned to the stretching and bending vibration of hydroxyls resulting from the presence of

bound and zeolitic water in sepiolite. [51]. The band at  $1425\text{ cm}^{-1}$  is attributed to CO of calcium carbonate, and the weaker band intensity revealed that the impurity was partly removed during the catalyst preparation, which is consistent with the XRD result [52]. Besides, there was no big difference for the FTIR spectra of the fresh and used Ag@Pt/sepiolite samples, implying the nice stability of the prepared catalyst.

### 3.2. Theoretical analysis of catalysts

The DFT calculations were employed for the theoretical analysis of Ag@Pt nanoparticles. The electron deformation density analy-

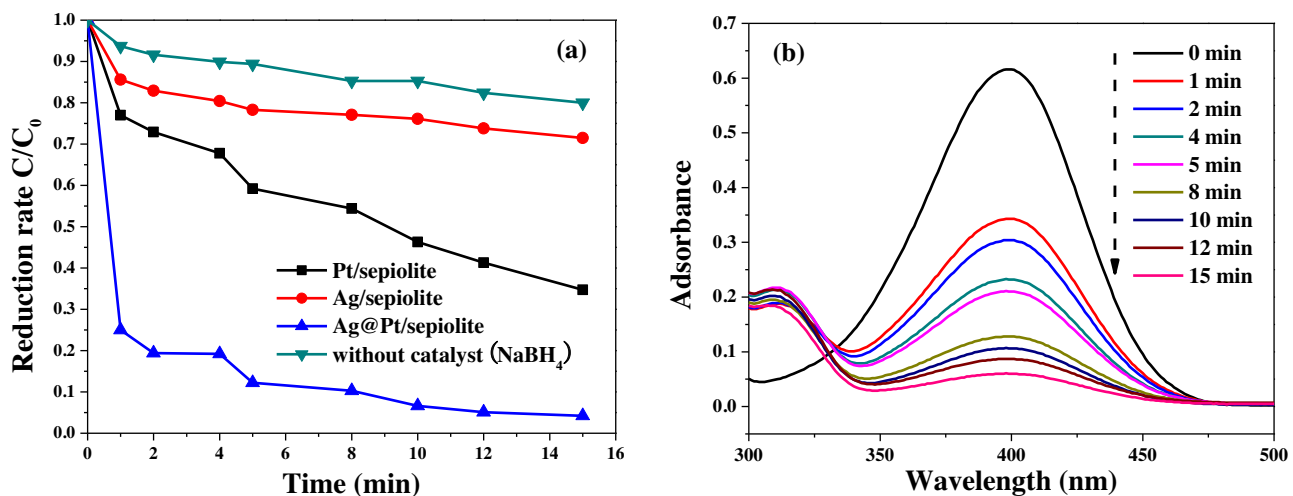


Fig. 9. The catalytic reduction of PNP over different catalysts (a) and the UV-vis absorption spectra of PNP reduced by  $\text{NaBH}_4$  over Ag@Pt/sepilite catalyst (b).

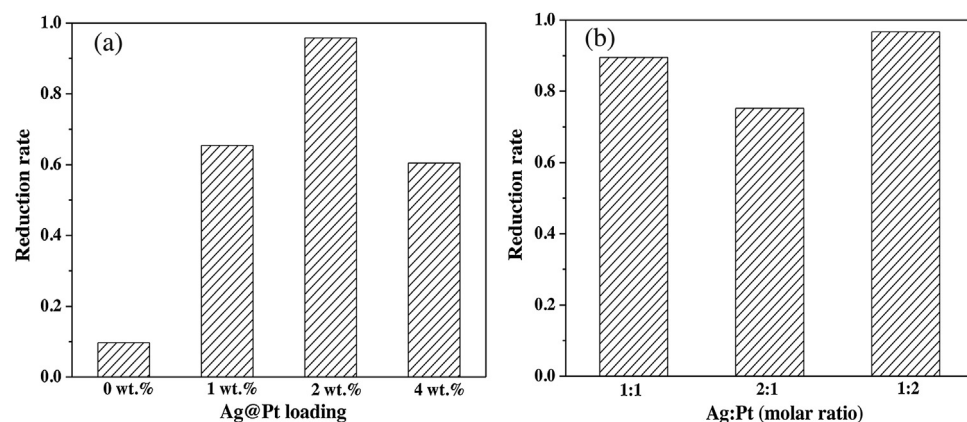


Fig. 10. The catalytic reduction of PNP on Ag@Pt/sepilite with different Ag@Pt loadings (a) and 2 wt.% Ag@Pt/sepilite with different Ag:Pt (b).

Table 2

Calculated Mulliken populations of Pt and Ag atoms in Ag@Pt nanoparticles compared with those in Pt and Ag nanoparticles, respectively.

Atomic Populations (Mulliken)		Ag@Pt	Pt	Ag
Ag	s	4.529	–	4.642
	p	9.025	–	8.941
	d	9.902	–	9.893
	Total	23.456	–	23.477
	Charge	0.087	–	0.046
Pt	s	5.462	5.409	–
	p	12.322	12.310	–
	d	14.311	14.279	–
	f	7.000	7.000	–
	Total	39.094	38.997	–
	Charge	–0.189	0.005	–

sis shown in Fig. 7 indicates that electrons are accumulated in Pt atom region with respect to Ag atom region at the interfaces of Pt shells and Ag cores [53,54]. Mulliken population analysis summarized in Table 2 also shows that the atomic population of Pt became more negative than that of Ag after the coating of Pt shells on Ag cores [32,55]. The results signified the charge transfer from Ag atoms to Pt atoms due to the higher electro-negativity of Pt (2.28) than that of Ag (1.93), which is compatible with the experimental characterization.

Fig. 8a–c shows that the total density of states (TDOS) of Ag, Ag@Pt and Pt nanoparticles is mainly composed of *s*- and *d*-orbitals in the energy level range. The TDOS of Ag@Pt nanoparticles at Fermi energy ( $E_F$ ) is much higher than that of Ag nanoparticles, demonstrating that the catalytic activity of Ag@Pt nanoparticles would be enhanced because of the lower stability of core-shell structure [56–58]. Moreover, the *s* band of Ag cores in Ag@Pt nanoparticles shifted to lower energy region compared with that in Ag nanoparticles, and *d* band of Pt shells has the opposite trend with the *s* band of Ag cores (Fig. 8d–e). It's also displayed that the *s*-orbitals of Ag cores (at –6.1, –5.3, –2.9, –2.5, –0.1, 0.7 and 1.4 eV) interacted with *d*-orbitals of Pt shells (at –5.7, –5.1, –2.9, –2.5, –0.8, –0.1 and 1.4 eV) [30,59]. These results denote the strong *s*-*d* hybridization and the charge redistribution between Ag cores and Pt shells, which contributed to the unique electronic structure of Ag@Pt nanoparticles.

### 3.3. Catalytic reduction of nitrophenols

#### 3.3.1. Catalytic reduction of PNP

The catalytic performance of Ag@Pt/sepilite catalyst for the reduction of PNP with  $\text{NaBH}_4$  was investigated in comparison with monometallic catalysts. As shown in Fig. 9a, the reduction rate of PNP to PAP by  $\text{NaBH}_4$  without catalyst is only 20% in 15 min, and the reduction rate of PNP to PAP by  $\text{NaBH}_4$  could reach over 95% on Ag@Pt/sepilite catalyst in the same time. However, the reduction rate of PNP to PAP by  $\text{NaBH}_4$  over Pt/sepilite and Ag/sepilite is 65% and 30%, respectively, indicating that the catalytic activities of

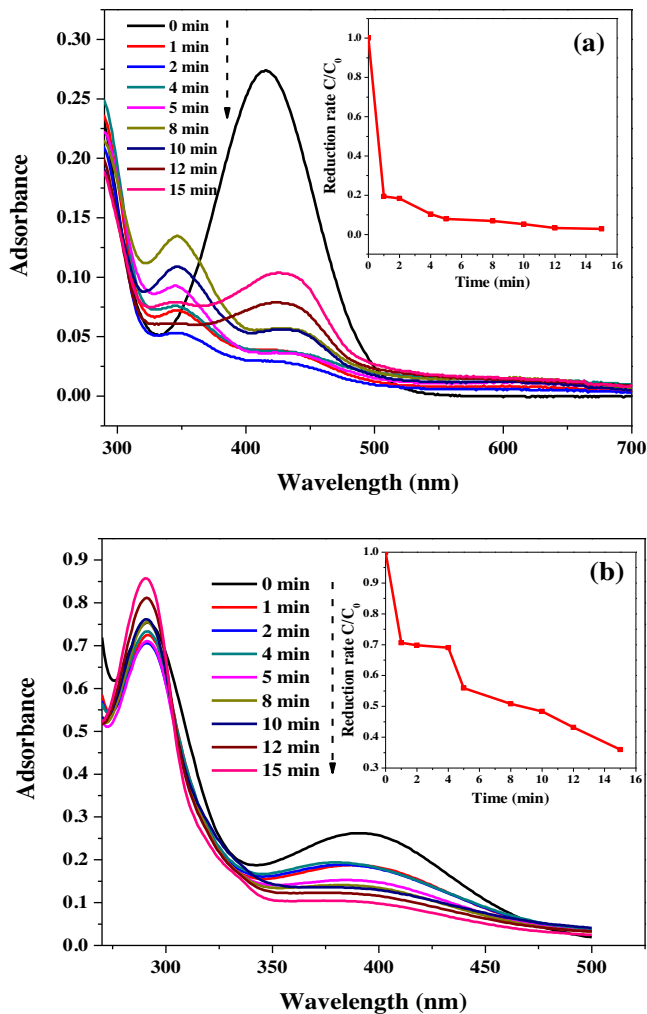


Fig. 11. The catalytic reduction of ONP (a) and MNP (b) on Ag@Pt/sepoltite catalyst.

Ag@Pt/sepoltite catalyst preceded those of monometallic catalysts under identical conditions. Fig. 9b displays the UV-vis absorption spectra of the PNP reduction with  $\text{NaBH}_4$  over Ag@Pt/sepoltite catalyst. PNP aqueous solution exhibited a peak at 400 nm in the presence of  $\text{NaBH}_4$ , corresponding to the characteristic peak of  $-\text{NO}_2$  in PNP [60]. A new peak at 315 nm, associated with  $-\text{NH}_2$  of PAP, appeared and increased with the addition of Ag@Pt/sepoltite catalyst, which demonstrates that the toxic PNP pollutant in water had been rapidly and efficiently reduced to valuable PAP under the acceleration of Ag@Pt/sepoltite catalyst [61].

**3.3.1.1. Effect of Ag@Pt loading.** The effect of Ag@Pt nanoparticles loading contents on the catalytic performance of Ag@Pt/sepoltite was investigated through the catalytic reduction of PNP to PAP. As can be seen in Fig. 10a, 2 wt.% Ag@Pt/sepoltite catalyst showed the largest catalytic reduction rate (96%, 15 min), followed by 0 and 1 wt.% Ag@Pt/sepoltite catalysts, which only partly catalyzed the reduction of PNP in same time due to less of reactive sites on Ag@Pt nanoparticles. In addition, the catalytic reduction rate of PNP by 4 wt.% Pt/sepoltite catalyst was much smaller than that by 2 wt.% one, which results from the decrease of reactive sites on agglomerated Ag@Pt nanoparticles and the blocking of pores and tunnels in sepoltite [62]. Therefore, the optimal Ag@Pt nanoparticles loading content for the catalytic reduction of PNP is 2 wt.% in this study.

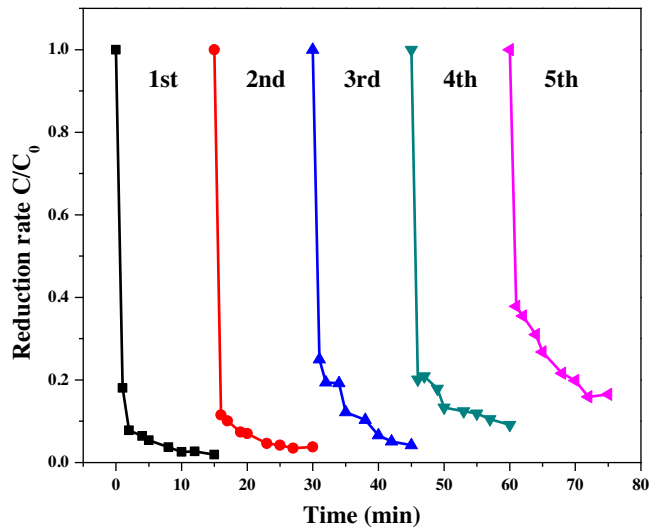


Fig. 12. Stability of Ag@Pt/sepoltite catalyst toward the catalytic reduction of PNP.

**3.3.1.2. Effect of Ag: Pt.** The effect of Ag: Pt on the catalytic performance of Ag@Pt/sepoltite was investigated through the catalytic reduction of PNP to PAP. Fig. 10b shows that the catalytic reduction rate of PNP on 2 wt.% Ag@Pt/sepoltite with Ag: Pt = 1:1, 2:1 and 1:2 were 90%, 70% and 97%, respectively. The enhanced catalytic performance of Ag@Pt/sepoltite with increasing Pt molar ratio is attributed to lower interaction energy of Pt than that of Ag according to d-band theory, and the prevention of Ag leaching by Pt shells [15]. However, the material cost of Pt is much higher than that of Ag. In order to decrease Pt consumption and enhance catalytic performance, 2 wt.% Ag@Pt/sepoltite with Ag: Pt = 1:1 was selected as the optimal catalyst in this study.

### 3.3.2. Catalytic reduction of ONP and MNP

The catalytic reduction of ONP and MNP (isomers of PNP) over Ag@Pt/sepoltite catalyst were investigated and shown in Fig. 11a–b. The catalytic reduction rate of ONP with  $\text{NaBH}_4$  in the presence of Ag@Pt/sepoltite catalyst could reach 97% within 15 min. The UV-vis absorption spectra during the catalytic reduction of ONP into OAP (Ortho-aminophenol) exhibited that the absorption peaks shifted from 414 nm to 346 nm, indicating that  $-\text{NO}_2$  of ONP was gradually reduced to  $-\text{NH}_2$  of OAP under the acceleration of Ag@Pt/sepoltite catalyst [63].

The catalytic reduction rate of MNP with  $\text{NaBH}_4$  in the presence of Ag@Pt/sepoltite catalyst could reach 70% within 15 min, which is lower than that of PNP and ONP under identical conditions due to the weaker electrophilicity of MNP in the absence of conjugative effect compared with PNP and ONP [61]. The UV-vis absorption spectra during the catalytic reduction of MNP into MAP (Meta-aminophenol) exhibited that the absorption peaks shifted from 394 nm to 290 nm, indicating that  $-\text{NO}_2$  of MNP was gradually reduced to  $-\text{NH}_2$  of MAP under the acceleration of Ag@Pt/sepoltite catalyst [64].

### 3.3.3. Catalytic stability

Fig. 12 shows the stability of Ag@Pt/sepoltite composite for the catalytic reduction of PNP. It is apparent from Fig. 12 that the catalytic reduction ability of the sample only decreased a little bit even after 5 repeated cycles. It means that the as-prepared sample has a high stability for the catalytic reduction of nitrophenols, which is consistent with the characterization results of XPS and FTIR. The stable and efficient performance of Ag@Pt/sepoltite catalyst ensures the high efficiency and low cost in practical wastewater treatment.

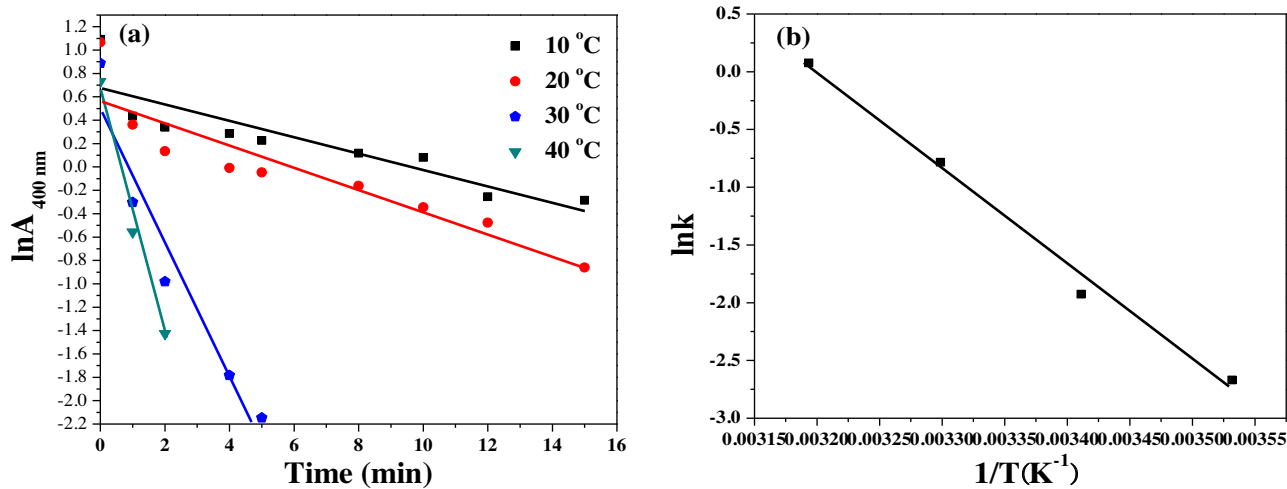
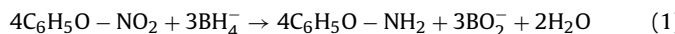


Fig. 13. (a) Plot of time versus  $\ln A_{400\text{nm}}$  by Ag@Pt/sepilolite at different temperatures; (b) Arrhenius plot of  $\ln k$  vs  $(1/T)$ .

### 3.4. Reaction kinetics of catalytic reduction

The reducing reaction of PNP to PAP with  $\text{NaBH}_4$  is could be described as Eq. (1). It's a thermodynamically favorable process due to the electrochemical potential of PNP/PAP ( $0.76 \text{ V}_{\text{SCE}}$ ) lower than that of  $\text{H}_3\text{BO}_3/\text{BH}_4^-$  ( $1.33 \text{ V}_{\text{SCE}}$ ), but a kinetically restricted reaction without the acceleration of catalysts [15].



$$\ln(C_0/C_t) = k_{\text{app}}t \Leftrightarrow \ln A_t = kt \quad (2)$$

$$k_{\text{app}} = Ae^{-E_a/RT} \Leftrightarrow \ln k = \ln A - E_a/RT \quad (3)$$

Langmuir-Hinshelwood model was adopted to analyze the kinetic process of catalytic reduction of PNP, and the kinetic reaction rate ( $k$ ) could be evaluated by a pseudo-first-order kinetics (Eq. (2)) because of the presence of excessive  $\text{NaBH}_4$ , and estimated from the plot of  $\ln A_{400\text{nm}}$  vs the reaction time ( $A_{400\text{nm}}$  is the absorbance at 400 nm) [65]. Fig. 13a exhibits that kinetic reaction rate ( $k$ ) of catalytic reduction of PNP over Ag@Pt/sepilolite catalyst at 10 °C, 20 °C, 30 °C and 40 °C is estimated to be  $0.07 \text{ min}^{-1}$ ,  $0.15 \text{ min}^{-1}$ ,  $0.46 \text{ min}^{-1}$  and  $1.08 \text{ min}^{-1}$ , respectively, which are comparable to other bimetallic catalysts for the catalytic reduction of PNP [10,66]. The apparent activation energy ( $E_a$ ) could be obtained from the Arrhenius equation (Eq. (3)) and determined by the plot of  $\ln k$  vs  $1/T$ , the value of  $E_a$  is  $69.02 \text{ kJ/mol}$  calculated from the slope ( $-E_a/R$ ,  $R$  is ideal gas constant) in Fig. 13b [67]. These results demonstrate that Ag@Pt/sepilolite catalyst could be expected to act as promising treatment for nitrophenols wastewater due to its high catalytic activity.

### 3.5. Catalytic reduction mechanism

A proposed mechanism for the catalytic reduction of nitrophenols with  $\text{NaBH}_4$  over Ag@Pt/sepilolite catalyst was presented in Fig. 14 according to the above results and previous works [68,69]. Firstly, the presence of  $\text{NaBH}_4$  in nitrophenols solution resulted in the deprotonation of nitrophenols to nitrophenolate ions. Secondly, nitrophenolate ions were adsorbed on surface of Ag@Pt/sepilolite catalyst through sepilolite nanofibers with large surface area and high porosity, and attached on the surface of Ag@Pt nanoparticles via nitro groups. Finally, electrons generated from the reaction of  $\text{BH}_4^-$  and  $\text{H}^+$  transferred to nitrophenolate ions through the unique electronic structure of Ag@Pt nanoparticles, and nitrophenolate ions received electrons to form aminophenols. The excellent catalytic performance of Ag@Pt/sepilolite catalyst for the reduction

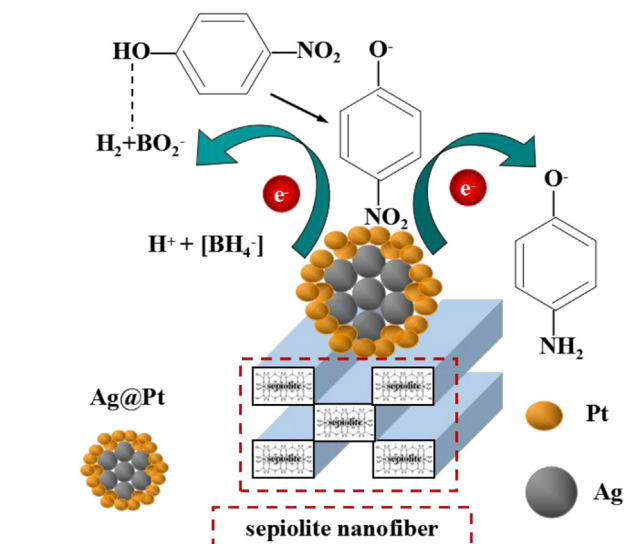


Fig. 14. Proposed catalytic mechanism of PNP reduction on Ag@Pt/sepilolite catalyst with  $\text{NaBH}_4$ .

of nitrophenols is ascribed to the large surface area of sepilolite nanofibers and the unique electronic structure of core-shell Ag@Pt nanoparticles.

### 4. Conclusions

Ag@Pt/sepilolite catalysts were expectably prepared through a simple successive reduction method and exhibited excellent catalytic performance for the reduction of nitrophenols. core-shell Ag@Pt nanoparticles were highly dispersed on sepilolite nanofibers, and charge redistribution and *s-d* hybridization between Ag cores and Pt shells resulted in the unique electronic structure of Ag@Pt/sepilolite catalysts. The catalytic reaction of nitrophenol reduction with excessive  $\text{NaBH}_4$  follows a pseudo-first-order kinetic equation, and Ag@Pt/sepilolite catalyst exhibits comparable kinetic reaction rate to other bimetallic catalysts. The catalytic reduction rate of nitrophenols with  $\text{NaBH}_4$  over 2 wt.%Ag@Pt/sepilolite catalyst (Ag: Pt = 1: 1) could reach 96% within 15 min, which was much superior to those of solely Ag and Pt deposited sepilolite. Moreover, it still presented a good stability even after 5 cycles. The stable and efficient catalytic property

of Ag@Pt/sepiolite catalyst is primarily ascribed to the large surface area and high porosity of nanofibrous sepiolite and core-shell structure of Ag@Pt nanoparticles, promoting the adsorption of nitrophenols in water and the electron transfer from  $\text{BH}_4^-$  to nitrophenols through the unique electronic structure, respectively.

## Acknowledgments

This work was supported by National Program on Key Basic Research Project of China (973 Program) 2013CB632402, NSFC (No.51472194), the NSF of Hubei Province (2016CFA078) and the Self-determined and Innovative Research Funds of Wuhan University of Technology (2015-zy-077).

## References

- [1] S. Pandey, S.B. Mishra, *Carbohydr. Polym.* 113 (2014) 525–531.
- [2] P. Cañizares, C. Sáez, J. Lobato, M.A. Rodrigo, *Ind. Eng. Chem. Res.* 43 (2004) 1944–1951.
- [3] E. Marais, T. Nyokong, *J. Hazard. Mater.* 152 (2008) 293–301.
- [4] H. Ma, H. Wang, C. Na, *Appl. Catal. B: Environ.* 163 (2015) 198–204.
- [5] L. Tao, Z. Zhu, F. Li, *Colloids Surf. A: Physicochem. Eng. Asp.* 425 (2013) 92–98.
- [6] C. Chu, Z. Su, *Langmuir* 30 (2014) 15349–15350.
- [7] Y.W. Lee, N.H. Kim, K.Y. Lee, K. Kwon, M. Kim, S.W. Han, *J. Phys. Chem. C* 112 (2008) 6717–6722.
- [8] Z. Dong, X. Le, C. Dong, W. Zhang, X. Li, J. Ma, *Appl. Catal. B: Environ.* 162 (2015) 372–380.
- [9] S. Alayoglu, B. Eichhorn, *J. Am. Chem. Soc.* 130 (2008) 17479–17486.
- [10] S.K. Ghosh, M. Mandal, S. Kundu, S. Nath, T. Pal, *Appl. Catal. A: Gen.* 268 (2004) 61–66.
- [11] T. Wu, L. Zhang, J. Gao, Y. Liu, C. Gao, J. Yan, *J. Mater. Chem. A* 1 (2013) 7384–7390.
- [12] H.-D. Kim, H.J. Park, T.-W. Kim, K.-E. Jeong, H.-J. Chae, S.-Y. Jeong, C.-H. Lee, C.-U. Kim, *Int. J. Hydrogen Energy* 37 (2012) 8310–8317.
- [13] D. Zhao, Y.-H. Wang, B. Yan, B.-Q. Xu, *J. Phys. Chem. C* 113 (2009) 1242–1250.
- [14] A. Aristizábal, S. Contreras, N.J. Divins, J. Llorca, F. Medina, *Appl. Catal. B: Environ.* 127 (2012) 351–362.
- [15] L. Jiang, W. Zhu, C. Wang, W. Dong, L. Zhang, G. Wang, B. Chen, C. Li, X. Zhang, *Appl. Catal. B: Environ.* 180 (2016) 344–350.
- [16] Z. Dong, X. Le, Y. Liu, C. Dong, J. Ma, *J. Mater. Chem. A* 2 (2014) 18775–18785.
- [17] C. Du, H. Yang, *J. Colloid Interface Sci.* 369 (2012) 216–222.
- [18] P. Praus, M. Turicová, M. Karliková, L. Kvítek, R. Dvorský, *Mater. Chem. Phys.* 140 (2013) 493–498.
- [19] N. Yuan, G. Zhang, S. Guo, Z. Wan, *Ultrason. Sonochem.* 28 (2016) 62–68.
- [20] C. Serna, J.L. Ahlrichs, J.M. Serratosa, *Clay Clay Miner.* 23 (1975) 452–457.
- [21] F.M. Bautista, J.M. Campelo, D. Luna, J. Luque, J.M. Marinas, *Appl. Catal. A: Gen.* 325 (2007) 336–344.
- [22] G. Zhang, Q. Xiong, W. Xu, S. Guo, *Appl. Clay Sci.* 102 (2014) 231–237.
- [23] M. Uğurlu, M.H. Karaoğlu, *Chem. Eng. J.* 166 (2011) 859–867.
- [24] Y. Zhang, D. Wang, G. Zhang, *Chem. Eng. J.* 173 (2011) 1–10.
- [25] K.-i. Shimizu, R. Maruyama, S.-i. Komai, T. Kodama, Y. Kitayama, *J. Catal.* 227 (2004) 202–209.
- [26] I. Küncel, S. Sener, *Ultrason. Sonochem.* 17 (2009) 250–257.
- [27] B. Delley, *J. Chem. Phys.* 113 (2000) 7756–7764.
- [28] B. Delley, *J. Chem. Phys.* 92 (1990) 508–517.
- [29] H.C. Genuino, M.S. Seraji, Y. Meng, D. Valencia, S.L. Suib, *Appl. Catal. B: Environ.* 163 (2015) 361–369.
- [30] B.B. Xiao, Y.F. Zhu, X.Y. Lang, Z. Wen, Q. Jiang, *Sci. Rep.* 4 (2014) 5205.
- [31] S.N. Datta, C.S. Ewig, J.R. van Wazer, *Chem. Phys. Lett.* 57 (1978) 83–89.
- [32] J. Sui, X. Wang, P. An, *Comput. Theor. Chem.* 1028 (2014) 98–105.
- [33] H.M. Lee, M. Ge, B.R. Sahu, P. Tarakeshwar, K.S. Kim, *J. Phys. Chem. B* 107 (2003) 9994–10005.
- [34] J.A. Rodriguez, S. Ma, P. Liu, J. Hrbek, J. Evans, M. Pérez, *Science* 318 (2007) 1757–1760.
- [35] H. Liu, W. Chen, C. Liu, Y. Liu, C. Dong, *Microporous Mesoporous Mater.* 194 (2014) 72–78.
- [36] M.P.S. Krekeler, S. Guggenheim, *Appl. Clay Sci.* 39 (2008) 98–105.
- [37] J. Cao, M. Guo, J. Wu, J. Xu, W. Wang, Z. Chen, *J. Power Sources* 277 (2015) 155–160.
- [38] C. Li, Y. Yamauchi, *Phys. Chem. Chem. Phys.* 15 (2013) 3490–3496.
- [39] K. Kim, K.L. Kim, K.S. Shin, *J. Phys. Chem. C* 115 (2011) 23374–23380.
- [40] X. Cao, N. Wang, Y. Han, C. Gao, Y. Xu, M. Li, Y. Shao, *Nano Energy* 12 (2015) 105–114.
- [41] J. Shi, *Chem. Rev.* 113 (2013) 2139–2181.
- [42] K.S.W. Sing, *Pure Appl. Chem.* 54 (1982) 2201–2218.
- [43] M. Barrera-Vargas, J. Valencia-Rios, M.A. Vicente, S.A. Korili, A. Gil, *J. Phys. Chem. B* 109 (2005).
- [44] J.T. Rajamathi, M.F. Ahmed, N. Ravishankar, C. Nethravathi, M. Rajamathi, *Solid State Sci.* 11 (2009) 1270–1274.
- [45] G. Leblanc, G. Chen, G.K. Jennings, D.E. Cliffler, *Langmuir* 28 (2012) 7952–7956.
- [46] M. Zhu, P. Chen, W. Ma, B. Lei, M. Liu, *Appl. Mater. Interfaces* 4 (2012) 6386–6392.
- [47] J. Yang, J. Yang, J.Y. Ying, *ACS Nano* 6 (2012) 9373–9382.
- [48] J. Yang, J.Y. Lee, T.C. Deivaraj, H.-P. Too, *Langmuir* 19 (2003) 10361–10365.
- [49] E. Sabah, M.S. Celik, *J. Colloid Interface Sci.* 251 (2002) 33–38 (36).
- [50] Y. Gao, H. Gan, G. Zhang, Y. Guo, *Chem. Eng. J.* 217 (2013) 221–230.
- [51] M. Alkan, G. Tekin, H. Namli, *Microporous Mesoporous Mater.* 84 (2005) 75–83.
- [52] A. Özcan, A.S. Özcan, *J. Hazard. Mater.* 125 (2005) 252–259.
- [53] X.H. Yang, H.T. Fu, K. Wong, X.C. Jiang, A.B. Yu, *Nanotechnology* 24 (2013) 415601.
- [54] S. Chen, S. Sun, B. Lian, Y. Ma, Y. Yan, S. Hu, *Surf. Sci.* 620 (2014) 51–58.
- [55] A. Staykov, T. Nishimi, K. Yoshizawa, T. Ishihara, *J. Phys. Chem. C* 116 (2012) 15992–16000.
- [56] O.R. Inderwildi, S.J. Jenkins, D.A. King, *Surf. Sci.* 601 (2007) L103–L108.
- [57] L. Hong, H. Wang, J. Cheng, X. Huang, L. Sai, J. Zhao, *Comput. Theor. Chem.* 993 (2012) 36–44.
- [58] Y. Jia, C. Belin, M. Tillard, L. Lacroix-Orio, D. Zitoun, G. Feng, *Inorg. Chem.* 46 (2007) 4177–4186.
- [59] Q. Meng, S. Wang, Y. Shen, B. Yan, Y. Wu, X. Ma, *Appl. Surf. Sci.* 292 (2014) 117–127.
- [60] J.-H. Noh, R. Meijboom, *Appl. Catal. A: Gen.* 497 (2015) 107–120.
- [61] V.K. Gupta, N. Atar, M.L. Yola, Z. Üstündag, L. Uzun, *Water Res.* 48 (2014) 210–217.
- [62] V. Belova, H. Möhwald, D.G. Shchukin, *Langmuir* 24 (2008) 9747–9753.
- [63] H. Liu, Q. Yang, *J. Mater. Chem.* 21 (2011) 11961–11967.
- [64] Q. Shi, M. Chen, G. Diao, *Electrochim. Acta* 114 (2013) 693–699.
- [65] L. Qiu, Y. Peng, B. Liu, B. Lin, Y. Peng, M.J. Malik, F. Yan, *Appl. Catal. A: Gen.* 413–414 (2012) 230–237.
- [66] B. Lai, Y. Zhang, Z. Chen, P. Yang, Y. Zhou, J. Wang, *Appl. Catal. B: Environ.* 144 (2014) 816–830.
- [67] A.M. Kalekar, K.K.K. Sharma, A. Lehoux, F. Audonnet, H. Remita, A. Saha, G.K. Sharma, *Langmuir* 29 (2013) 11431–11439.
- [68] F.-h. Lin, R.-a. Doong, *Appl. Catal. A: Gen.* 486 (2014) 32–41.
- [69] Y. Hao, X. Shao, B. Li, L. Hu, T. Wang, *Mater. Sci. Semicond. Process.* 40 (2015) 621–630.